



Vulnerability of Primary Productivity and Its Carbon Use Efficiency to Unfavorable Climatic Conditions in Jambi Province, Indonesia

Ummu Ma'rufah¹, Tania June^{1*}, Ashehad Ashween Ali², Akhmad Faqih¹, Yonny Koesmaryono¹, Christian Stiegler² & Alexander Knohl²

¹Agrometeorology Division, Department of Geophysics and Meteorology, Faculty of Mathematics and Natural Sciences, IPB University, Campus IPB Dramaga, Indonesia

²Bioclimatology, Faculty of Forest Science, University of Göttingen, Göttingen, Germany

*E-mail: taniajune@apps.ipb.ac.id

Abstract. Climatic conditions and land cover play crucial roles in influencing the process of carbon uptake through vegetation. This study aimed to analyze the effect of climate variability on carbon uptake of four different land covers in Jambi Province, Indonesia. The four land cover types studied were: forest, shrub, grass, and irrigated soybean, based on Community Land Model version 5. Forest was found to have the highest net primary production (NPP) compared to the other land covers. Seasonal climate variability showed no major effect on NPP and gross primary production (GPP). However, GPP and NPP experienced significant declines during El Niño Southern Oscillation (ENSO), particularly in 2015. Carbon use efficiency (CUE = NPP/GPP) was also affected by ENSO, where CUE decreased during El Niño, particularly in October and November with an increased number of days without rainfall. In addition, the difference between latent (LE) and sensible heat (H) flux, denoted as (LE-H), decreased from August to November. This difference was highly correlated with NPP. This result indicates that when water supply is low, stomata will close, thereby reducing photosynthesis and transpiration, and allocating more of the available energy to sensible heat flux rather than latent heat flux.

Keywords: CUE latent heat; ENSO; land use; NPP; sensible heat.

1 Introduction

Vegetation on the land surface influences the absorbance of atmospheric carbon, where carbon is fixed by plants into organic compounds through photosynthesis. This carbon flux is referred to as gross primary production (GPP) [1]. In terrestrial ecosystems, GPP is the largest carbon flux, which activates several ecosystem functions, including growth and respiration [2]. The part of GPP used for plant respiration is known as autotrophic respiration (R_a), while the part used for the formation of the stem, leaf, root, and fruit biomass is referred to as net primary production (NPP) [3]. In terrestrial ecosystems, NPP is the main component of

energy and mass transformation. In addition, terrestrial NPP provides a major portion of the food supply essential for human wellbeing [4].

Carbon uptake in terrestrial ecosystems is influenced by land cover type and environmental conditions such as climate [5]. Each land cover type has a different ability in terms of carbon absorbance [6]. Forests help mitigate climatic change by sequestering carbon from the atmosphere and storing it in tree biomass. Tropical forests store 212 gigaton carbon per year in their trees alone [7]. Furthermore, forests are an important component of the terrestrial carbon cycle, as they typically store more carbon than other land cover types [8]. Based on a study in China, forest-stored carbon is 32%, 300%, and 150% higher than that of grassland, shrubland, and cropland, respectively [9]. An observation from tropical Amazon shows that carbon sequestration in tropical forests starts to decline because of an increase in tree mortality [10,11]. From 1983 to 2011, carbon sequestration in the Amazon tropical forest decreased at a rate of $-0.034 \text{ Mg C ha}^{-1} \text{ year}^{-2}$ [11]. Meanwhile, shrubs have been found to grow faster than trees and play a strategic role in carbon sequestration [12]. Two hypotheses have been formulated to explain the faster growth of shrubs compared to trees. Firstly, shrubs with several stems ensure that even if one dies, the plant will continue to grow and flourish [12]. Secondly, short shrub stems have three structural characteristics that outperform tall tree stems with regard to survivability [12]. According to Sha *et al.* (2020) in [13], grasses are also crucial in the global carbon cycle and they also contribute to carbon sequestration. Each land cover type has a positive or negative impact on the carbon balance. Therefore, analyzing the relationship between land cover type and carbon sequestration is necessary.

Climatic conditions also affect the process of carbon sequestration in plants, particularly temperature and rainfall [14]. This condition is due to different types of vegetation showing different growth patterns and differences in the response of carbon allocation to water and heat stress [15]. Under unfavorable climatic conditions such as drought, plants generally carry out more respiration, whereas the allocation of carbon for plant biomass decreases [16]. 'Unfavorable climatic conditions' refers to a state outside the optimum that causes a decrease in productivity. According to Cavaleri *et al.* (2017) [17], tropical rainforests experienced a 7% increase in respiration and a 10% reduction in GPP during El Niño in 1998. However, according to Zhang *et al.* (2016) [18], forests do not show a significant change in leaf area index (LAI) under drought. However, non-forest land covers such as grasses and shrubs show rapid changes in canopy characteristics because of water stress [15,19].

In Indonesia, extremely dry conditions often occur during El Niño [20]. El Niño causes dry seasons to be 1 to 5 months longer than normal, which often leads to forest fires [21,22]. Within Indonesia, Jambi Province in Sumatra is one of the

regions with a particularly strong decrease in rainfall during El Niño [22]. Drought also has a significant impact on carbon sequestration during this period in Jambi Province. According to Stiegler *et al.* (2019) [23], El Niño led to an 86% decrease in carbon sequestration of oil palm plantations in 2015. However, the impact of climatic variability on carbon sequestration is still unknown for other land covers in Jambi Province.

The expansion of oil palm plantations, rubber plantations, dryland agriculture, transmigration, mining activities, and forest fires is the driving factor of deforestation in Jambi [24,25]. The conversion of forest to oil palm and rubber plantations causes significant losses in plant and animal lives and a significant change in microclimate [26]. However, based on remote sensing data in Jambi, forests usually do not directly become oil palm and rubber plantations; transition plants such as grass, shrub, and dryland agriculture also arise [27]. Therefore, this study aimed to analyze the differences between primary production in forests and some transition plants, including grasses, shrubs, and soybean plants. It also aimed to determine the influence of climatic variability on primary production and carbon use efficiency (CUE) of four land covers. CUE is defined as the proportion of carbon used for growth with carbon absorbed by vegetation through photosynthesis [28]. CUE is an important regulator for carbon sequestration in the ecosystem [29]. In the present study, primary productivity was simulated using Community Land Model version 5 (CLM5).

2 Method

2.1 Model description and setting

This study used the Community Earth System Model, which is a coupled community model that includes ocean, atmosphere, land, rivers, sea ice, and land ice [30]. Only the land component, CLM5, was activated in the present study [31]. In default CLM5, vegetation characteristics such as LAI are prescribed from satellite phenology (SP), while vegetation states are predicted in the biogeochemistry (BGC) module [31]. Based on the simulation of biomass, LAI, ecosystem carbon pools and fluxes, energy exchange, and terrestrial water storage, CLM5 has better performance than previous versions [31]. The present study used point simulations at a tropical rain forest site, i.e., the Harapan Forest 1 (HF1) plot of the Ecological and Socioeconomic Function of Tropical Lowland Rainforest Transformation Systems (EFForTS, Figure 1) [26]. Harapan Forest is a tropical forest in lowland Jambi that has experienced intensive area loss [32].

The simulations were divided into three parts, namely, spin up, historical conditions, and current conditions. This study used the CLM5-BGC module, so spin up was required. Spin up is a standard procedure used in CLM5 to attain

carbon, water, and energy equilibrium [31]. The spin up procedure included accelerated spin up as well as normal spin up. In accelerated mode, carbon and nitrogen, which decompose slowly, are exposed to acceleration [31,33]. Normal spin up used a pre-industrial CO₂ concentration (284.7 ppm). During the accelerated spin up procedure, meteorological data from 1942 to 1971 were repeated for a 300-year simulation to reach equilibrium between the carbon and nitrogen pools. This was followed by 300 years of normal spin up.

The historical simulation covered the period from 1951 to 2000. The current simulation covered the period from 2001 to 2015 and used a transient CO₂ concentration and broadleaf evergreen tropical forest plant functional types (PFTs). We performed a clear cut [34] in 2000 and replaced forest with shrub, grass, and soybean. Then, we performed the current simulation with forest, shrub, grass, and soybean. The PFTs of broadleaf evergreen shrub and C3 grass were used for shrub and grass, respectively. Soybean was represented by the PFTs of irrigated tropical soybean. The planting period of soybean was set from November to February. In this simulation, the vegetation state, such as height, stem, and LAI, was prognostically computed through the activation of the biogeochemistry (BGC) model. The vegetation parameters were not obtained from Jambi Province, but the default data from the model were used.

CLM5 can simulate biogeophysical and BGC processes in land. The biogeophysical process in CLM5 measures the surface energy balance using the following equation:

$$S\uparrow - S\downarrow + L\uparrow - L\downarrow = \lambda E + H + G, \quad (1)$$

where $S\uparrow$ ($S\downarrow$) is the upwelling (downwelling) solar radiation; $L\uparrow$ ($L\downarrow$) is the upwelling (downwelling) longwave radiation; λ is the latent heat of vaporization; E is the evaporation; H is the sensible heat flux; and G is the ground heat flux. The value of the left-side equation is called net radiation (Rn). Solar radiation absorbed by vegetation and ground was calculated based on incident direct beam and diffuse solar flux. Sensible heat flux (H) and latent heat flux (LE) were processed using the following equations [35]:

$$H = -\rho_{\text{atm}} c_p ((\theta_{\text{atm}} - \theta_s)/r_{\text{ah}}), \quad (2)$$

$$LE = -\rho_{\text{atm}} ((q_{\text{atm}} - q_s)/r_{\text{aw}}), \quad (3)$$

where ρ_{atm} is the density of air (kg m^{-3}); c_p is the specific heat capacity of air ($\text{J kg}^{-1} \text{K}^{-1}$); $\theta_{\text{atm}} - \theta_s$ is the difference between the potential temperature of the atmosphere at reference height $z_{\text{atm},x}$ (m) and the surface (K); $q_{\text{atm}} - q_s$ is the difference between the specific humidity of the atmosphere at reference height $z_{\text{atm},x}$ (m) and the surface (kg kg^{-1}); r_{ah} and r_{aw} are the aerodynamic resistance

values for sensible heat and water vapor transfer, respectively. In the biogeochemical process, CLM5 solves carbon and nitrogen cycling based on the natural vegetation, crop, or soil. This cycling varies depending on the specific PFT types. GPP, NPP, and respiration were calculated in the biogeochemical model of CLM5. The detail process and formula are explained in Lawrence *et al.* (2018) [35].

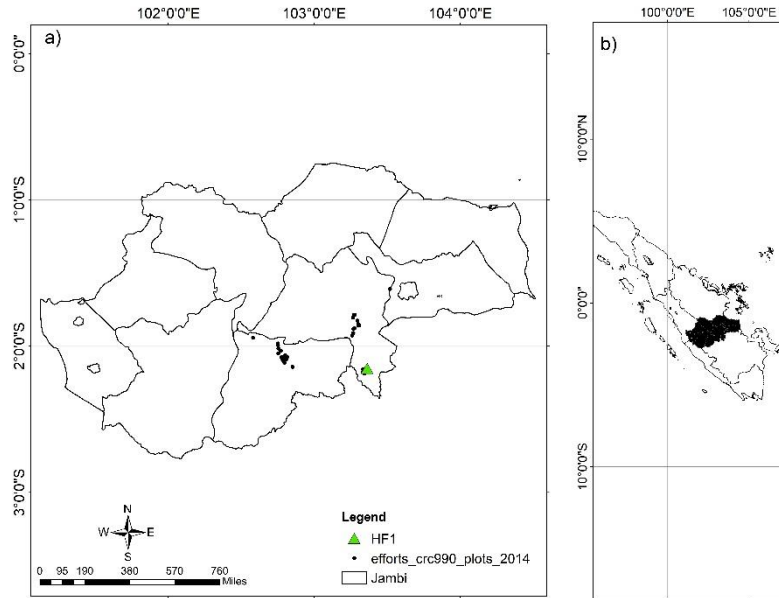


Figure 1 Study area for the EFForTS project in the HF1 plot, Jambi Province.

2.2 Model Evaluation

The Pearson correlation was used to test the output model [36]:

$$r = \frac{\sum (x_i - \bar{x})(y_i - \bar{y})}{\sqrt{\sum (x_i - \bar{x})^2 \sum (y_i - \bar{y})^2}}, \quad (4)$$

where r is the correlation coefficient; x_i is the value from observation; \bar{x} is the mean of the observation values; y_i is the value of the model output, and \bar{y} is the mean of the model output values. This study only evaluated two variables, namely, net radiation and latent heat flux, because the plot in the study area only had a meteorological station. Net radiation was calculated from observation data using the following equation:

$$R_n = (1 - \alpha)R_s + \sigma T^4 (0.34 - 0.14\sqrt{e_a}) (1.35 \frac{R_s}{R_{s0}} - 0.35), \quad (5)$$

where α is the albedo; T is the hourly air temperature (K); σ is the Stefan–Boltzmann constant (2.043×10^{-10} MJ K⁻⁴ m⁻² h⁻¹); R_s is the solar radiation (MJ m⁻² h⁻¹); R_{so} is the clear sky radiation (MJ m⁻² h⁻¹), and e_a is the actual vapor pressure (kPa). In addition, the latent heat flux was determined by multiplying energy for evaporation (L) with evapotranspiration. Potential evapotranspiration (ET_0) was defined on the basis of the FAO Penman–Monteith method [37]:

$$ET_0 = \frac{0.408 \Delta R_n + \gamma \frac{37}{(T+273)} U_2 (e_s - e_a)}{\Delta + \gamma(1 + 0.34 U_2)}, \quad (6)$$

where e_s is the saturation vapor pressure (kPa); U_2 is the average hourly wind speed at 2 m (m s⁻¹); e_a is the actual hourly vapor pressure (kPa); γ is the psychrometric constant (kPa °C⁻¹), and Δ is the slope curve of vapor-pressure–air temperature (kPa °C⁻¹).

2.3 Data

CRUNCEP atmospheric forcing data for 1951–2015 were used, i.e., solar radiation, air temperature, total precipitation rate, wind speed, specific humidity, and pressure [38]. The spatial and temporal resolution of the data were 0.5° x 0.5° and 6-hourly, respectively. In addition, data on aerosol and concentration of CO₂ were used, which were taken from <https://svn-ccsm-inputdata.cgd.ucar.edu/trunk/inputdata>. Soil texture information, i.e., clay and sand fraction in the top 200 cm, was obtained from Hassler *et al.* (2015) [39]. The information about El Niño and its intensity was obtained from <https://ggweather.com/enso/oni.htm>. We used data from the 2002, 2006, 2009, and 2015 El Niño events for analysis.

2.4 Data Analysis

Climatic variability analysis was conducted to reveal seasonal and annual variations. These seasonal and annual variations focused on the dry and wet seasons and El Niño years, respectively. Furthermore, the dry and wet seasons were determined based on the climatological data of precipitation. The dry/wet season was defined by monthly rainfall below/above 150 mm/month [40]. The average data within the period of 2001–2015 were also compared with those of El Niño years to understand the impact of El Niño on carbon uptake. The difference between latent and sensible heat fluxes (LE-H) represented climatic condition, while NPP, GPP, and Ra indicated that these fluxes were related to the carbon cycle. Moreover, the carbon uptake of different land-use cover types was analyzed using CUE:

$$CUE = NPP/GPP \quad (7)$$

3 Result

3.1 Model Evaluation

The model was evaluated to analyze its performance in capturing real conditions. CLM5 was evaluated based on two output data, i.e., net radiation and latent heat flux. The plot in the study area only had a meteorological station, which did not measure carbon flux. Thus, the output model was only evaluated based on net radiation and latent heat flux. The FAO Penman–Monteith method was used to compute the LE observations. With a p -value below 0.05, the coefficients of correlation between the model output and the observation data for net radiation and latent heat flux were 0.89 and 0.87, respectively (Figure 2), indicating that the CLM5 output almost matched the observation data. Therefore, based on the coefficient correlation value, CLM5 performed well in simulating the biogeophysical process in land.

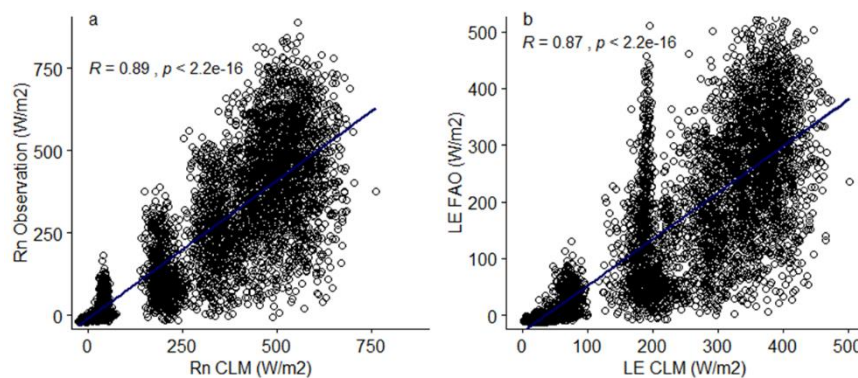


Figure 2 Coefficient correlation between the hourly model output and the observational data for net radiation (a) and latent heat fluxes (b).

3.2 Climate Variables in Jambi

Rainfall in Jambi Province varies seasonally. According to Aldrian & Dwi Susanto (2003) [41], Jambi has an equatorial type of rainfall, where the peak of the rainy season occurs twice per year, in the periods March-April and November-December. The dry season in Jambi Province occurs from June to September (Figure 3a). This season is characterized by monthly rainfall below 150 mm/month [40]. The mean air temperature in Jambi is approximately 27.2 °C to 28.5 °C (Figure 3b). Air temperatures rise in May and October. Solar radiation also has two peaks, which occur in the periods March-April and September-October (Figure 3c). Jambi is located near the equator, so the sun is above the area twice. When the sun is above the equator, incoming solar radiation in Jambi increases.

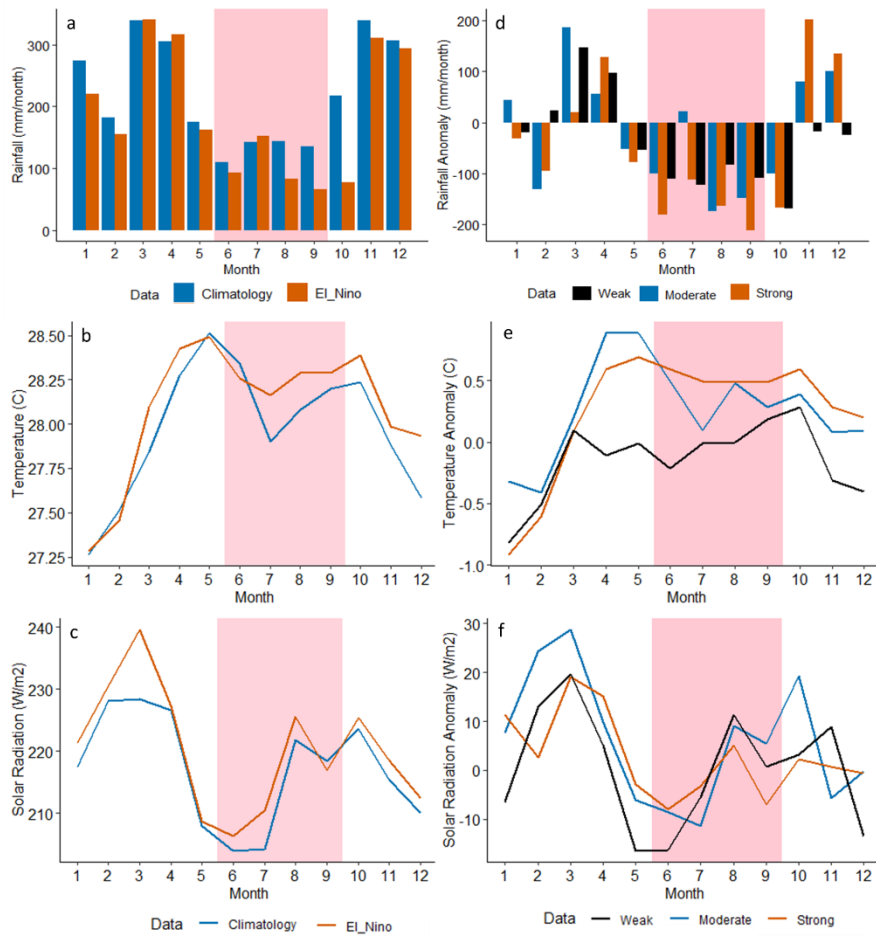


Figure 3 Left side is climatological and El Niño data of CRUNCEP consisting of rainfall (a), temperature (b), and incoming solar radiation (c) at the HF1. The right side is the anomaly of rainfall (d), temperature (e), and incoming solar radiation (f) at the HF1 during weak (2006), moderate (2002), and strong (2015) El Niño. The shaded area shows the dry season.

Jambi Province is an area that is strongly influenced by El Niño, where the dry season becomes drier than in normal conditions [22]. The average annual rainfall in Jambi is 2,183 mm, which decreases to 1,658 mm during El Niño. During El Niño, rainfall in Jambi decreases from May to October (Figures 3a and 3d). The impact of El Niño on rainfall in Jambi depends on its strength (Figure 3d). Strong El Niño events as occurred in 2015 have a more pronounced impact than weak and moderate El Niño. Rainfall in Jambi can reduce up to 200 mm/month during El Niño.

El Niño affects not only rainfall but also other climate variables such as temperature and solar radiation. The mean temperature increased during El Niño by up to 0.25 °C, particularly in the dry season (Figure 3b). The increasing temperature during strong El Niño is greater than that during weak and moderate El Niño. Sometimes it can create hotspots that trigger forest fires in parts of Jambi Province [42]. Solar radiation increases during El Niño up to 30 W/m², particularly during moderate El Niño (Figure 3c). However, solar radiation during strong El Niño has a smaller increase than during medium and weak El Niño, and sometimes the value also decreases (Figure 3f). During the strong El Niño event in 2015, a forest fire occurred that caused Jambi to be covered by smoke [42]. According to Stiegler *et al.* (2019) [41], during El Niño in 2015, incoming solar radiation decreased by 35% compared to normal conditions. Diffuse radiation became primary shortwave radiation for almost two months, from mid-September to mid-November, with a fraction increase from 0.21 in normal conditions to 0.99 during the haze period.

3.3 Differences in Primary Production in Forest, Grass, Shrub, and Soybean Land Cover

The four land cover types differ in their ability to absorb carbon, with GPP being larger in forest, grass, and shrub compared to soybean (Figure 4). This because forests, grasses, and shrubs are evergreen plants. The C-uptake or GPP from these three land covers is high, i.e. approximately 2.7 kgC/m²/year. However, most of the carbon absorbed is used for plant respiration. Meanwhile, only a small amount of carbon is stored in the form of plant biomass. Forest stores 1.04 kgC/m²/year as biomass, while the remaining 1.65 kgC/m²/year is used for respiration. Grass and shrub store 1.08 and 0.73 kgC/m²/year as biomass, while the remaining 1.6 and 2.03 kgC/m²/year are used for respiration, respectively. The respiration of shrub was found to be 0.38 kgC/m²/year higher than that of forest because of its faster growth than trees [12]. In the case of soybean, the carbon produced by photosynthesis is mostly stored in the form of plant and fruit biomass. Moreover, the carbon sequestration in soybean was 0.03-0.37 kgC/m²/year lower than that in the other three land covers over 15 years. In seasonal crops, a non-planting period from March to September was identified, during which the land is open with no carbon absorption by plants.

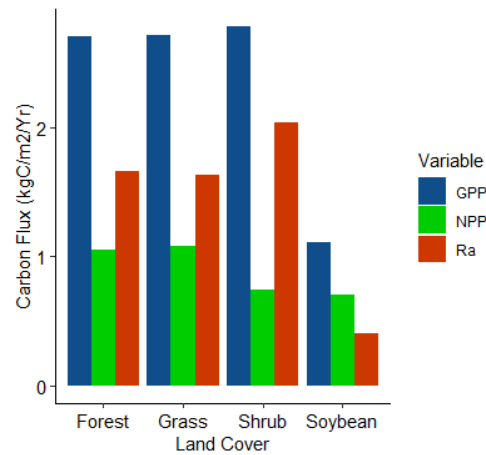


Figure 4 Estimated yearly average carbon flux from CLM5 output in forest, grass, shrub, and soybean from 2001-2015.

3.4 Effect of Climate Variability on Surface Energy Balance

Water availability in land can be identified based on biogeophysical processes, particularly from the partition of net radiation into sensible heat flux and latent heat flux. Sensible heat flux is energy for heating up air, whereas latent heat flux is energy for evapotranspiration. The amount of allocation energy in these two components is complementary, which indicates that biogeophysically, the allocation of energy will be prioritized for latent heat flux in areas with sufficient water. Therefore, latent heat flux is always greater than sensible heat flux when water is available.

The difference between latent heat flux and sensible heat flux (LE-H) in forest, shrub, grass, and soybean (during planting periods) is high, i.e., approximately 90-120 W/m² during normal conditions (Figure 5a). This occurs because Jambi has high annual rainfall [25,26], therefore, water is always available throughout the year. However, LE-H declines during El Niño. The decline of LE-H in forest, shrub, grass, and soybean was approximately 20-50 W/m², and occurred particularly from September to October (Figure 5). Among the land covers, the decline of LE-H in forest was the lowest. During September to November, LE-H in forest decreased by approximately 21 W/m², followed by grass, shrub, and soybean by approximately 29, 36, and 44 W/m², respectively.

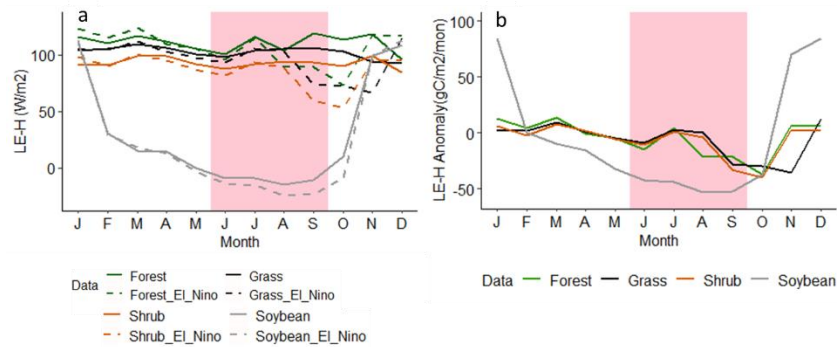


Figure 5 Difference between latent heat flux and sensible heat flux (LE-H) estimated from CLM5 output for forest, grass, shrub, and soybean (a) and its anomaly during El Niño (b). The solid line represents the average monthly data from 2001-2015, while the dashed line represents the average of El Niño. The shaded area shows the dry season.

In general, forest had higher LE-H than shrub, grass, and soybean in normal conditions and during El Niño. Forest has higher surface roughness than shrub, grass, and soybean. Given their rough surface, forest canopies are better at dissipating heat than aerodynamically smooth land covers [43] such as grass, shrub, and soybean. Therefore, sensible heat flux for forest is lower and LE-H is higher than for smooth land covers. Forests with a dense canopy can reduce runoff. In addition, forest trees can improve soil infiltration and groundwater recharge [44]. Therefore, forests can conserve water and will not immediately experience a water shortage in the case of rainfall deficiency. During drought, forests with deep roots can take water from deeper soil layers [45], so the LE-H decrease is low. In contrast, grass, shrub, and soybean cannot conserve water. In addition, these three land-use types have shorter roots than forests. Therefore, the LE-H decrease for grass, shrub, and soybean was greater than for forest. Soybean showed the highest decrease in LE-H from September to October. During this period, the land becomes bare, so more of the available energy will be used for warming up the surface, and LE-H will decline significantly.

3.5 Effect of Climate Variability on Primary Productivity

Carbon sequestration that occurs terrestrially is influenced by several factors, some of which are climate variables such as temperature, rainfall, and radiation [46,47]. Solar radiation decreases, temperature increases, and rainfall decreases can reduce carbon sequestration [48]. In addition, LE-H has an impact on carbon sequestration. Changes in LE-H are correlated with NPP for all land cover types during El Niño (Table 1), indicating the close control of water and CO₂ fluxes.

Table 1 Correlation between NPP and LE-H from CLM5 output during El Niño.

No	Land cover	Correlation between NPP and LE-H
1	Forest	0.76
2	Grass	0.60
3	Shrub	0.89
4	Soybean	0.89

In general, carbon sequestration in forest, shrub, and grass was not significantly affected by seasonal climatic variability (Figure 6). The dry season did not significantly impact the decrease in carbon absorption, as GPP, NPP, and Ra were relatively constant throughout the year. The monthly average GPP, NPP, and Ra values for forest were approximately 222.2, 86.2, and 135.9 gC/m²/month, respectively. Meanwhile, the monthly average GPP, NPP, and Ra values for grass (shrub) were approximately 222.5 (216.5), 88.9 (60.8), and 133.5 (155.7) gC/m²/month, respectively. However, for soybean, the GPP, NPP, and Ra values were high during the growing season in October-February. The monthly average GPP, NPP, and Ra values during the growing season were approximately 218.4, 139, and 79.1 gC/m²/month, respectively. In contrast, during the non-planting period from March to August, the GPP, NPP, and Ra values became zero.

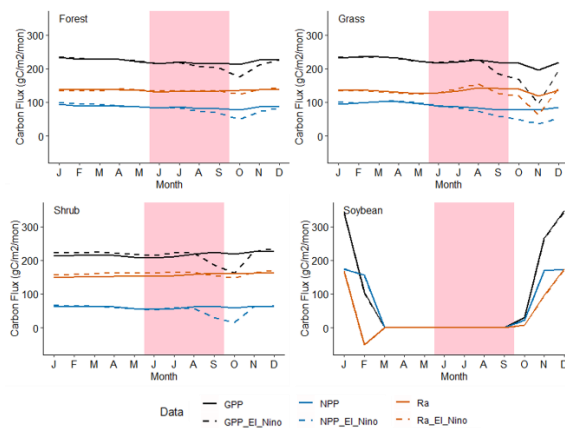


Figure 6 Carbon flux from CLM5 output for forest, grass, shrub, and soybean. The solid line represents the average of the monthly data from 2001 to 2015, while the dashed line represents the average for El Niño. The shaded area shows the dry season.

During El Niño, carbon sequestration in forest, grass, and shrub significantly decreased from August to November (Figure 6). Meanwhile, the peak of the decrease occurred in October and November. Therefore, further analysis of the impact of El Niño on primary production focused on October to November.

Between 2001 and 2015, the average net carbon flux, or NPP, in October-November for forest, grass, shrub, and soybean land cover was 82, 77, 61, and 96 gC/m²/month, respectively. During El Niño, the average net carbon flux, or NPP, in October-November for forest, grass, and shrub decreased to 51, 22, and 27 gC/m²/month, respectively.

The net carbon flux for forest decreased by 38%, followed by shrub (55%) and grass (71%). Grass had a higher decrease in net carbon uptake than forest and shrub. According to Breshears *et al.* (2016) [49], drought conditions that are drier and hotter reduce water availability in grassland systems and trigger grass mortality. Shrub is more adaptive than grass in drought conditions [49], although the decrease in carbon flux is also high. Under dry conditions and high temperatures, the physiological condition of grass and shrub will deteriorate. Stomatal conductance will decrease to suppress the transpiration rate of the plants [50,51]. In addition, the decrease in stomatal conductance decreases photosynthesis, as indicated by a reduction in GPP. Forest had the lowest decrease in net carbon flux. This could be influenced by the availability of water in this ecosystem. Based on the LE-H value, the decrease in water availability for forest during El Niño was lower than for grass and shrub. Therefore, stomatal conductance for forest, which affects photosynthesis, will remain higher than for grass and shrub. In soybean, the net carbon flux did not decrease because it used an irrigation system, so water was always supplied. Thus, a rainfall deficit over a longer period will not significantly affect carbon absorption through photosynthesis.

Moderate (2002), weak (2006), and strong (2015) El Niño events had different impacts on carbon sequestration in terms of GPP, NPP, and Ra (Figure 7). Carbon sequestration experienced a significant decline during the strong El Niño event in 2015 in all vegetation (Figure 7), as Jambi Province experienced extreme drought within this period [52,53]. Extreme drought indicates dry conditions caused by a long period of rainfall deficit. According to Ma'rufah *et al.* (2017) in [52], most regions in Indonesia, including Jambi, experienced extreme drought in 2015 based on the standardized precipitation index and vegetation health index. As mentioned above, during the strong El Niño event, a fire occurred that caused Jambi to be covered by smoke. This caused direct radiation entering the land surface to decrease and diffused radiation [23]. The decrease in radiation reaching the surface also inhibited photosynthesis, as carbon absorption was reduced [51].

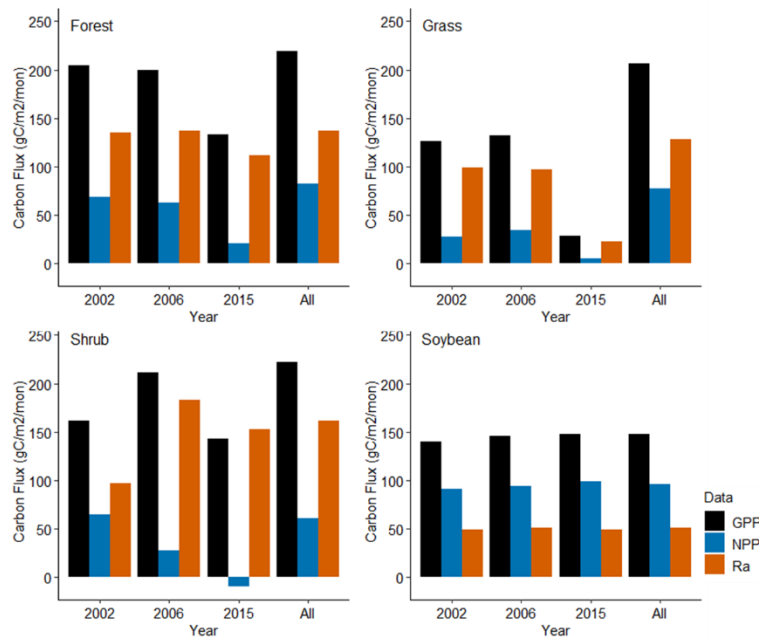


Figure 7 Average carbon flux from CLM5 output in October-November based on the 2001-2015 data, and moderate (2002), weak (2006), and strong (2015) El Niño.

3.6 CUE in Forest, Grass, Shrub, and Soybean Land Covers

Carbon use efficiency (CUE) is the ratio between NPP and GPP, which describes the proportion of assimilated carbon that is used for growth [28]. Among the four land covers, soybean had the highest CUE value during the planting period (Figure 8). The average CUE for soybean in the planting period was 0.77. This result indicates that most of the atmospheric carbon uptake was converted to plant biomass. Based on agricultural crop, a large amount of carbon is allocated to the harvested organ of the soybean during the reproduction phase [54]. CUE values were high in February, ahead of the harvest period. Forest, grass, and shrub had constant CUE values of 0.38, 0.39, and 0.29, respectively. This was due to the composition of plant biomass, which does not change as in agricultural crops [54].

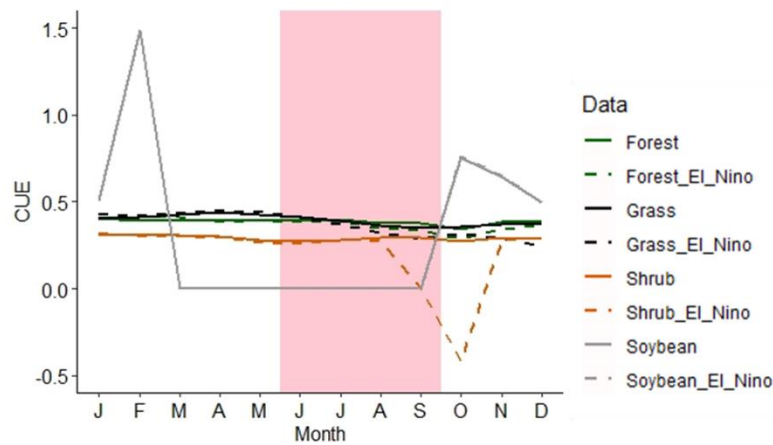


Figure 8 The carbon use efficiency (CUE = NPP/GPP) from the CLM5 output for forest, grass, shrub, and soybean. The solid line represents the average of the monthly data from 2001-2015, and the dashed line represents the average for El Niño. The shaded area shows the dry season.

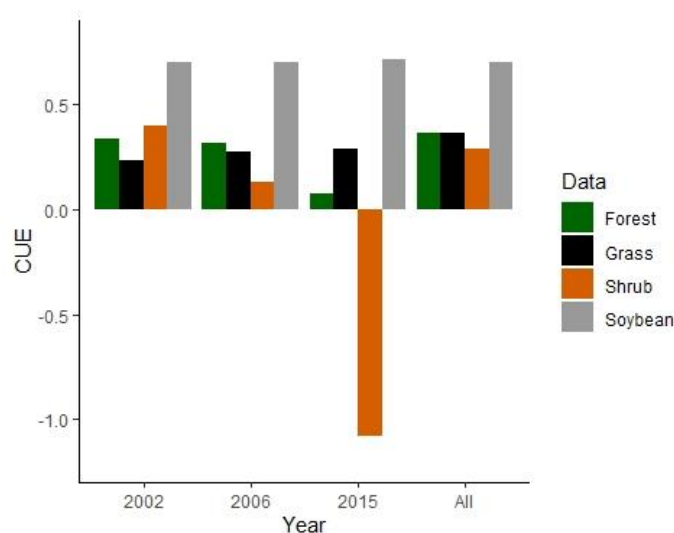


Figure 9 Average carbon use efficiency of the CLM5 output in October-November from the 2001-2015 and moderate (2002), weak (2006), and strong (2015) El Niño.

CUE is sensitive to changes in the environment such as temperature and water availability [28]. Seasonal climatic variability did not have a significant effect on CUE. Seasonal variability only caused a slight change in carbon sequestration [55]. This result indicates that no significant differences were observed in

environmental conditions between the dry and rainy seasons. However, CUE experienced a significant decline during El Niño. In general, the decline in CUE also occurred in October and November based on GPP and NPP.

During moderate and weak El Niño, the decline in CUE for forest and shrub was lower compared to that during strong El Niño (Figure 9). In forest (shrub), during moderate and weak El Niño, CUE was 0.33 and 0.31 (0.28 and 0.39), respectively, whereas during strong El Niño, CUE became 0.07 (−1.08). For grass and soybean, no significant difference was observed among weak, moderate, and strong El Niño. During El Niño, the CUE of grass and soybean was approximately 0.26 and 0.7, respectively.

Extreme drought decreased water availability during the strong El Niño event in 2015. This caused the GPP of plants to decrease. Among the four land covers, forest had the lowest CUE in 2015, even though it is better at conserving water (Figure 5). In addition, forests have greater biomass than grasses, shrubs, and soybean plants. Thus, the large decrease in CUE for forests during strong El Niño was due to high plant respiration, which led to low carbon allocation for biomass growth. Moreover, the negative CUE for shrub was due to a significant decrease in photosynthesis caused by stomatal closure, while plant respiration remained high.

This result led to a negative NPP and a significant decrease in CUE. In grass, extreme drought only slightly decreased CUE because grass does not have high biomass. Thus, decreasing photosynthesis is not followed by high respiration in grass. In soybean, CUE remained high during strong El Niño because water was always available because of irrigation. Based on this result, shrub is most affected by strong El Niño because it will serve as a carbon emitter in extreme drought conditions.

4 Discussion

Climate variability has a considerable impact on climate variables in Jambi Province. During El Niño, the dry conditions cause an increased air temperature (Figure 3e). In addition, there is more incoming solar radiation due to less cloud cover, except during forest fires, which cause atmosphere closure by smoke (Figure 3f). El Niño also significantly reduces rainfall from May to October (Figure 3d). Changes in climatic variables can affect the water balance (shown by LE-H) and carbon sequestration. LE-H, GPP and NPP decreased from August to November during El Niño. There was a time lag between reduction of rainfall and reduction of LE-H, GPP, and NPP. The overall amount of rainfall does not provide an appropriate indication of the water available to affect carbon flux [56,57]. Soil moisture is a better indicator for the water available to affect carbon

flux than rainfall [58]. In this study, water availability is indicated by LE-H as a partition of the surface energy balance depending on soil moisture [59,60]. LE-H has a high correlation with the net carbon flux and is a better indicator of the water available to affect carbon flux than rainfall.

Every land-use type responds differently to unfavorable climate conditions, as occur during El Niño. Forest is more tolerant to drought than grass and shrub. Forest can conserve water, so LE-H is still high in dry conditions. As a result, the net carbon flux does not decrease significantly during El Niño. In contrast, grass and shrub have low LE-H during the dry season, leading to a significant decrease in net carbon flux. During El Niño, LE-H for shrub is lower than for grass. However, grass has lower net carbon flux than shrub because low LE-H in grass occurs over a more extended period than in shrub. Soybean uses irrigation, so carbon flux for this land-use type is not affected by El Niño. Soybean has a higher CUE than the other land-use types because crop plants use most carbon absorption for plant biomass rather than for plant respiration. Based on carbon flux and CUE, forest is a land-use type that can adapt better to unfavorable climate conditions. Finally, it is crucial to protect forests from being degraded because, in the study area, the forests mostly turn to shrubs after fires, whereas shrubs are vulnerable to dry conditions.

The carbon flux analyzed in this study was simulation model output, which was not validated with data from measurements. Further, we used global data for atmospheric forcing in CLM5, because meteorological measurements in the study area only started in 2014. Therefore, it should be noted that the data presented in this study are estimates of actual values. However, this estimation of actual values can be used for preliminary analysis.

5 Conclusion

Carbon sequestration was strongly affected by climatic conditions, including rainfall, solar radiation, and temperature. These meteorological parameters varied seasonally, although the seasonal climatic variability did not have a major effect on GPP and NPP. During El Niño, the mean temperature increased by up to 0.25 °C, while the decrease in rainfall reached 200 mm/month. Incoming solar radiation can either increase or decrease. During El Niño, incoming solar radiation was high because of the absence of clouds in the sky. However, incoming solar radiation will decrease when forest fires occur, causing the atmosphere to be covered with smoke. This changing meteorological parameter could affect carbon flux. GPP and NPP significantly decreased during El Niño periods, which showed vulnerability to unfavorable climate conditions (long periods without rainfall, atmosphere covered with smog, and reduction of direct incoming radiation). Forest is more tolerant to drought compared to grass and

shrub. Meanwhile, soybean has more stable carbon absorption because water availability on the land was maintained through irrigation. Based on all four land cover types, GPP and NPP decreased during weak and moderate El Niño. Furthermore, the CUE was significantly affected by El Niño, particularly during the strong El Niño event in 2015. The CUE also experienced a decline during October and November. Based on energy partition, the difference between latent and sensible heat fluxes (LE-H) decreased between August and November. In addition, NPP and LE-H were positively correlated, indicating the close coupling of the water and carbon fluxes.

6 Acknowledgments

This research was funded by the Deutsche Forschungsgemeinschaft (DFG), project number 192626868–SFB 990, in the framework of the Collaborative German-Indonesian Research Center 990: Ecological and Socioeconomic Functions of Tropical Lowland Rainforest Transformation Systems (EFForTS). It was also partially funded by PMDSU, Directorate General of Higher Education, Ministry of National Education, Indonesia.

References

- [1] Beer, C., *Terrestrial Gross Carbon Dioxide Uptake: Global Distribution and Covariation with Climate*, Science (80-.), **329**(5993), pp. 834–838, Aug. 2010.
- [2] Ma, J., Yan, X., Dong, W. & Chou, J., *Gross Primary Production of Global Forest Ecosystems Has Been Overestimated*, Sci. Rep., **5**(1), pp. 1–9, Jun. 2015.
- [3] Pan, Y., *A Large and Persistent Carbon Sink in The World's Forests*, Science (80-.), **333**(6045), pp. 988–993, Aug. 2011.
- [4] Chapin, F.S., *Reconciling Carbon-Cycle Concepts, Terminology, And Methods*, Ecosystems, **9**(7). Springer, pp. 1041–1050, 17-Nov-2006.
- [5] Pan, S., *Modeling and Monitoring Terrestrial Primary Production in A Changing Global Environment: Toward A Multiscale Synthesis of Observation and Simulation*, Adv. Meteorol., **2014**, 2014.
- [6] Toru, T. & Kibret, K., *Carbon Stock Under Major Land Use/Land Cover Types of Hades Sub-Watershed, Eastern Ethiopia*, Carbon Balance Manag., **14**(1), p. 7, May 2019.
- [7] Malhi, Y., Baldocchi, D.D. & Jarvis, P.G., *The Carbon Balance of Tropical, Temperate and Boreal Forests*, Plant. Cell Environ., **22**(6), pp. 715–740, Jun. 1999.
- [8] Gray, A.N. & Whittier, T.R., *Carbon Stocks and Changes on Pacific Northwest National Forests and The Role of Disturbance, Management, and Growth*, For. Ecol. Manage., **328**, pp. 167–178, Sep. 2014.

- [9] Xu, L., *Carbon Storage in China's Terrestrial Ecosystems: A Synthesis*, Sci. Reports 2018 81, **8**(1), pp. 1–13, Feb. 2018.
- [10] Hubau, W., *Asynchronous Carbon Sink Saturation in African and Amazonian Tropical Forests*, Nature, **579**(7797), pp. 80–87, Mar. 2020.
- [11] Brienen, R.J.W., *Long-term decline of the Amazon Carbon Sink*, Nat. 2015 5197543, **519**(7543), pp. 344–348, Mar. 2015.
- [12] Götmark, F., Götmark, E. & Jensen, A.M., *Why be a shrub? A Basic Model and Hypotheses for the Adaptive Values of a Common Growth Form*, Frontiers in Plant Science, **7**, no. JULY2016. Frontiers Research Foundation, pp. 1095, 26-Jul-2016.
- [13] Sha, Z., Bai, Y., Lan, H., Liu, X., Li, R. & Xie, Y., *Can More Carbon Be Captured by Grasslands? A Case Study of Inner Mongolia, China*, Sci. Total Environ., **723**, pp. 138085, Jun. 2020.
- [14] Chen, Y. & Xiao, W., *Estimation of Forest NPP and Carbon Sequestration in the Three Gorges Reservoir Area, Using the Biome-BGC Model*, Forests, **10**(2), pp. 149, Feb. 2019.
- [15] Sippel, S., *Drought, Heat, and the Carbon Cycle: a Review*, Current Climate Change Reports, **4**(3). Springer, pp. 266–286, 01-Sep-2018.
- [16] Zhang, Y., *Climate-Driven Global Changes in Carbon Use Efficiency*, Glob. Ecol. Biogeogr., **23**(2), pp. 144–155, Feb. 2014.
- [17] Cavaleri, M.A., Coble, A.P., Ryan, M.G., Bauerle, W.L., Loescher, H.W. & Oberbauer, S.F., *Tropical Rainforest Carbon Sink Declines During El Niño As A Result of Reduced Photosynthesis And Increased Respiration Rates*, New Phytol., **216**(1), pp. 136–149, Oct. 2017.
- [18] Zhang, Y., Xiao, X., Zhou, S., Ciais, P., McCarthy, H. & Luo, Y., *Canopy And Physiological Controls of GPP During Drought and Heat Wave*, Geophys. Res. Lett., **43**(7), pp. 3325–3333, Apr. 2016.
- [19] Bai, Y., *Variation in Root:Shoot Ratios Induced the Differences Between Above and Belowground Mass-Density Relationships Along an Aridity Gradient*, Acta Oecologica, **36**(4), pp. 393–395, Jul. 2010.
- [20] Supari, Muharsyah, R. & Sopaheluwakan, A., *Mapping Drought Risk in Indonesia Related to El-Niño Hazard*, in AIP Conference Proceedings, **1730**(1), pp. 070001, 2016.
- [21] Edwards, R.B., Naylor, R.L., Higgins, M.M. & Falcon, W.P., *Causes Of Indonesia's Forest Fires*, World Dev., **127**, pp. 104717, Mar. 2020.
- [22] Khoir, A. N. U., Yuni, D., Atikah, R.N. & Safril, A., *The Influence of Strong El Niño to Seasonal Variability in Sumatera*, in AIP Conference Proceedings, **1987**(1), pp. 020029, 2018.
- [23] Stiegler, C., Mejjide, A., Fan, Y., Ali, A.A., June, T., & Knohl, A., *El Niño-Southern Oscillation (ENSO) Event Reduces CO₂ Uptake of an Indonesian Oil Palm Plantation*, Biogeosciences, **16**(14), pp. 2873–2890, Jul. 2019.
- [24] Rustiadi, E., Barus, B., Iman, L.S., Mulya, S.P., Pravitasari, A.E., &

- Antony, D., *Land Use and Spatial Policy Conflicts in a Rich-Biodiversity Rain Forest Region: The Case of Jambi Province, Indonesia*, Springer, Singapore, 2018, pp. 277–296, 2018.
- [25] F. Stolle, K. Chomitz, E. F. Lambin, and T. Tomich, *Land use and vegetation fires in Jambi Province, Sumatra, Indonesia*, For. Ecol. Manage., **179**, pp. 277–292, Jul. 2003.
- [26] Drescher, J., *Ecological and socio-economic functions across tropical land use systems after rainforest conversion*, Philos. Trans. R. Soc. B Biol. Sci., **371**(1694), pp. 20150275, May 2016.
- [27] Clough, Y., *Land-Use Choices Follow Profitability at The Expense of Ecological Functions In Indonesian Smallholder Landscapes.*, Nat. Commun., **7**, p. 13137, 2016.
- [28] Bradford, M.A. & Crowther, T.W., *Carbon Use Efficiency and Storage in Terrestrial Ecosystems*, New Phytol., **199**(1), pp. 7–9, Jul. 2013.
- [29] Chen Z. & Yu, G., *Spatial Variations and Controls of Carbon Use Efficiency In China’s Terrestrial Ecosystems*, Sci. Rep., **9**(1), pp. 1–10, 2019.
- [30] Danabasoglu, G., *The Community Earth System Model Version 2 (CESM2)*, J. Adv. Model. Earth Syst., **12**(2), p. e2019MS001916, Feb. 2020.
- [31] Lawrence, D.M., *The Community Land Model Version 5: Description of New Features, Benchmarking, and Impact of Forcing Uncertainty*, J. Adv. Model. Earth Syst., 2019.
- [32] Melati, D.N., *Carbon Emission Estimation Due To Land Cover Change in the Tropical Forest Landscape in Jambi Province*, J. Sains dan Teknol. Mitigasi Bencana, **14**(1), pp. 27, 2019.
- [33] X. Gao, A. Avramov, E. Saikawa, & C. A. Schlosser, *Emulation of Community Land Model Version 5 (CLM5) to Quantify Sensitivity of Soil Moisture to Uncertain Parameters*, J. Hydrometeorol., **22**(2), pp. 259–278, Feb. 2021.
- [34] Fan, Y., *A sub-canopy structure for simulating oil palm in the Community Land Model (CLM-Palm): Phenology, allocation and yield*, Geosci. Model Dev., **8**(11), pp. 3785–3800, 2015.
- [35] D. Lawrence, R. Fisher, C. Koven, K. Oleson, S. Swenson, and M. Vertenstein, *CLM5 Documentation*. Colorado: National Center for Atmosphere Research, 2018.
- [36] K. F. Weaver, V. Morales, S. L. Dunn, K. Godde, and P. F. Weaver, “Pearson’s and Spearman’s Correlation,” *An Introd. to Stat. Anal. Res.*, pp. 435–471, Aug. 2017.
- [37] R. G. Allen, L. S. Pereira, and D. Raes, “Crop evapotranspiration-Guidelines for computing crop water requirements-FAO Irrigation and drainage paper 56 Table of Contents,” 1998.
- [38] N. Viovy, “CRUNCEP Version 7 - Atmospheric Forcing Data for the

- Community Land Model.” Research Data Archive at the National Center for Atmospheric Research, Computational and Information Systems Laboratory, Boulder, CO, 2018.
- [39] E. Hassler, M. D. Corre, A. Tjoa, M. Damris, S. R. Utami, & E. Veldkamp, *Soil Fertility Controls Soil-Atmosphere Carbon Dioxide and Methane Fluxes in A Tropical Landscape Converted from Lowland Forest to Rubber and Oil Palm Plantations*, *Biogeosciences*, **12**(19), pp. 5831–5852, 2015.
- [40] T. Wati, S. Kusumaningtyas, & E. Aldrian, *Study of Season Onset Based on Water Requirement Assessment*, *IOP Conf. Ser. Earth Environ. Sci.*, **299**, 2019.
- [41] Aldrian, E. & Dwi Susanto, R., *Identification of Three Dominant Rainfall Regions Within Indonesia and Their Relationship to Sea Surface Temperature*, *Int. J. Climatol.*, **23**(12), pp. 1435–1452, 2003.
- [42] L. B. Prasetyo, A. H. Dharmawan, F. T. Nasdian, and S. Ramdhoni, “Historical Forest fire Occurrence Analysis in Jambi Province During the Period of 2000 – 2015: Its Distribution & Land Cover Trajectories,” *Procedia Environ. Sci.*, **33**, pp. 450–459, Jan. 2016.
- [43] Burakowski, E., *The role of surface roughness, albedo, and Bowen ratio on ecosystem energy balance in the Eastern United States*, *Agric. For. Meteorol.*, **249**, pp. 367–376, Feb. 2018.
- [44] Ellison, D., *Trees, forests and water: Cool insights for a hot world*, *Glob. Environ. Chang.*, **43**, pp. 51–61, Mar. 2017.
- [45] Lüttschwager, D. & Jochheim, H., *Drought Primarily Reduces Canopy Transpiration of Exposed Beech Trees and Decreases the Share of Water Uptake from Deeper Soil Layers*, *For.* **11**(5), pp. 537, May 2020.
- [46] Templer, P.H., *Biogeochemistry: Limits on Carbon Uptake By Plants*, *Nature Climate Change*, **3**(3). Nature Publishing Group, pp. 184–185, 26-Mar-2013.
- [47] T. Tharammal, G. Bala, N. Devaraju, & R. Nemani, *A Review of The Major Drivers of The Terrestrial Carbon Uptake: Model-Based Assessments, Consensus, and Uncertainties*, *Environmental Research Letters*, **14**(9). Institute of Physics Publishing, pp. 093005, 09-Sep-2019.
- [48] A. Dai, J. C. Fyfe, S.-P. Xie, and X. Dai, *Decadal Modulation of Global Surface Temperature by Internal Climate Variability*, *Nat. Clim. Chang.*, **5**(6), pp. 555–559, 2015.
- [49] D. D. Breshears, A. K. Knapp, D. J. Law, M. D. Smith, D. Twidwell, & C. L. Wonkka, *Rangeland Responses to Predicted Increases in Drought Extremity*, *Rangelands*, **38**(4), pp. 191–196, Aug. 2016.
- [50] M. K. Bartletta, T. Klein, S. Jansen, B. Choat, & L. Sack, “The correlations and sequence of plant stomatal, hydraulic, and wilting responses to drought,” *Proc. Natl. Acad. Sci. U. S. A.*, vol. 113, no. 46, pp. 13098–13103, Nov. 2016.

- [51] D. Bonal, B. Burban, C. Stahl, F. Wagner, & B. Hérault, “The response of tropical rainforests to drought—lessons from recent research and future prospects,” *Ann. For. Sci.*, **73**(1), pp. 27–44, Mar. 2016.
- [52] U. Ma’Rufah, R. Hidayat, & I. Prasasti, “Analysis of relationship between meteorological and agricultural drought using standardized precipitation index and vegetation health index,” in *IOP Conference Series: Earth and Environmental Science*, 2017, vol. 54, no. 1.
- [53] Sari, F.N., June, T. & A. Knohl, *Dynamics of The Standardized Precipitation Evapotranspiration Index (SPEI) of An Oil Palm Plantation Area In Jambi Province, Indonesia*, in *IOP Conference Series: Earth and Environmental Science*, **187**(1), p. 12065, 2018.
- [54] P. Steduto, T. C. Hsiao, and E. Fereres, “On the conservative behavior of biomass water productivity,” *Irrig. Sci.*, vol. 25, no. 3, pp. 189–207, Mar. 2007.
- [55] U. Marufah, T. June, A. Faqih, A. A. Ali, C. Stiegler, and A. Knohl, *Implication of Land Use Change To Biogeophysical and Biogeochemical Processes in Jambi, Indonesia: Analysed Using CLM5*, *Terr. Atmos. Ocean. Sci.*, **32**(2), pp. 203–215, Apr. 2021.
- [56] Y. Tang, J. Jiang, C. Chen, Y. Chen, & X. Wu, *Rainfall pulse response of carbon fluxes in a temperate grass ecosystem in the semiarid Loess Plateau*, *Ecol. Evol.*, **8**(22), pp. 11179, Nov. 2018.
- [57] Zhang, R., *Impacts of Precipitation on Ecosystem Carbon Fluxes in Desert-Grasslands in Inner Mongolia, China*, *J. Geophys. Res. Atmos.*, **124**(3), pp. 1266–1276, Feb. 2019.
- [58] Green, J.K., *Large Influence of Soil Moisture On Long-Term Terrestrial Carbon Uptake*, *Nature*, **565**(7740), p. 476, Jan. 2019.
- [59] Schwingshackl, C., M. Hirschi, & S. I. Seneviratne, *Quantifying Spatiotemporal Variations of Soil Moisture Control on Surface Energy Balance and Near-Surface Air Temperature*, *J. Clim.*, **30**(18), pp. 7105–7124, Sep. 2017.
- [60] X. Liu, J. Xu, S. Yang, & Y. Lv, *Surface Energy Partitioning and Evaporative Fraction in a Water-Saving Irrigated Rice Field*, *Atmos.* **10**(2), pp. 51, Jan. 2019.